Supporting Information

Confined Quantum Dots in Nanoporous Glass Matrices for Tunable Photoluminescence and Optoelectronic Applications

Dongyuan Dai[a],[b],1, Peixi Cong[c],1, Rui Wang[a],1, Tiantian Yin[a],*, Yibo Wang[d], Pengwei Wang[a], Qi Yue[a], Ran Luo[a], Zixiao Xue[a], Chenfang Lin[b], Da Shi[d], Long Zhang[a], Anlian Pan[b],[e],* and Jin He[a],*

[a] Research Center of Infrared Optical Materials, Department of Advanced Laser and Optoelectronic Functional Materials, Shanghai Institute of Optics and Fine Mechanics, Chinese Academy of Sciences, Shanghai 201800, China

[b] Key Laboratory for Micro-Nano Physics and Technology of Hunan Province, State Key Laboratory of Chemo/Biosensing and Chemometrics, Hunan Institute of Optoelectronic Integration, College of Materials Science and Engineering, Hunan University, Changsha 410082, China.

[c] Department of Materials, University of Oxford, Parks Road, Oxford OX1 3PH, UK.

[d] School of Chemical and Environmental Engineering, Shanghai Institute of Technology, Shanghai 201418, China

[e] School of Physics and Electronics, Hunan Normal University, Changsha 410081, China.

1. These authors contributed equally to this work.

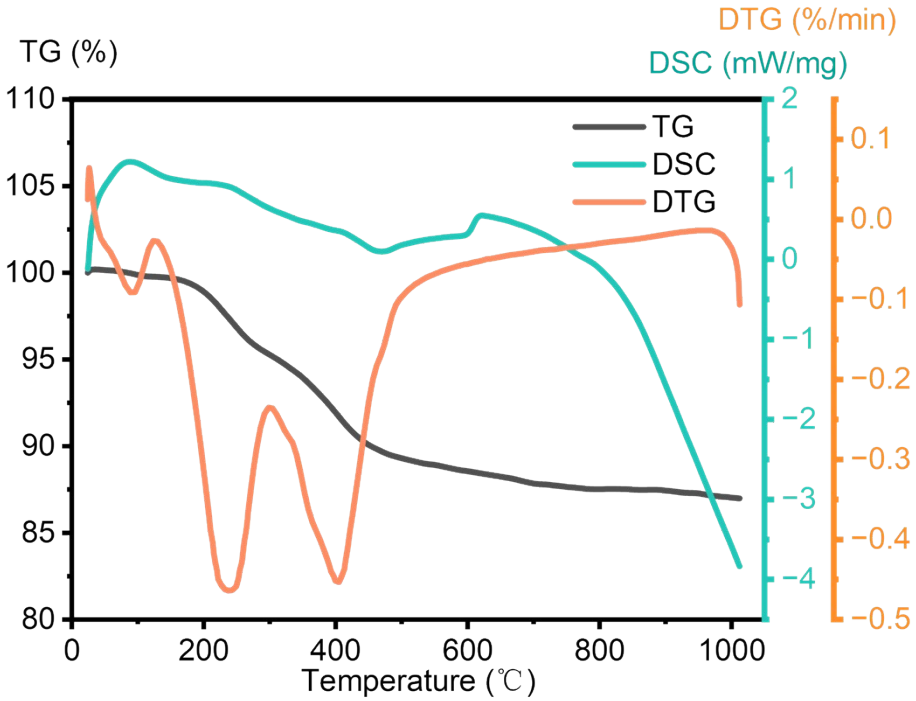

Figure S1. TG-DSC-DTG curves of the dried xerogel.

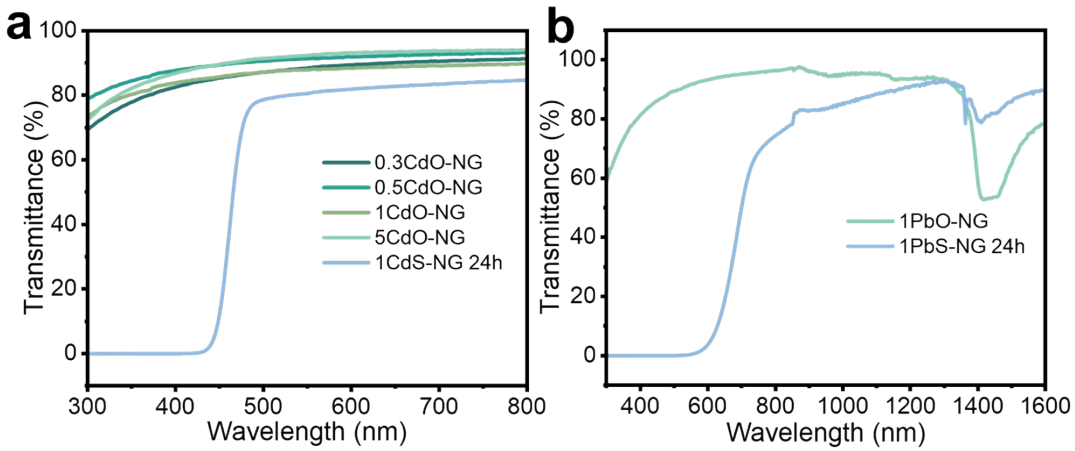

Figure S2. Optical transmittance spectrum of **(a)** 0.3/0.5/1/5CdO-NG and 1CdS-NG 24 h and **(b)** 1PbO-NG and 1PbS-NG 24 h.

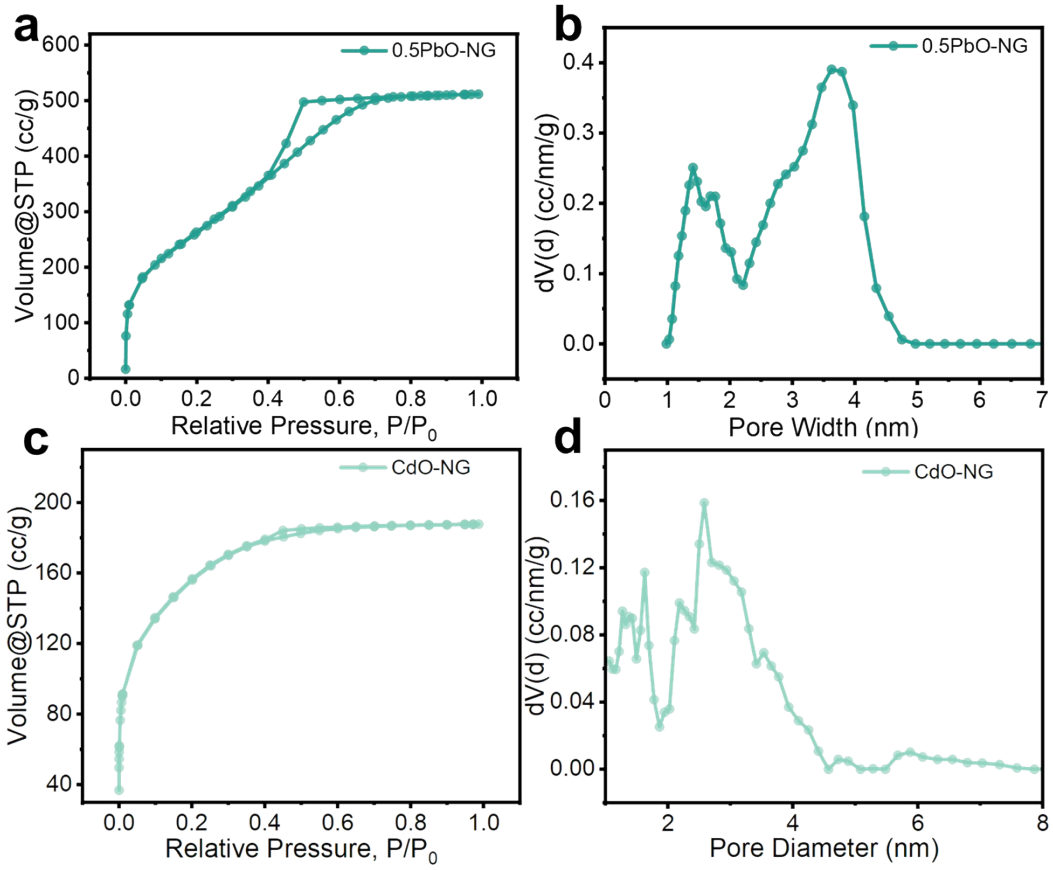

Figure S3. (a) Nitrogen adsorption-desorption isotherm diagram and **(b)** Pore diameter distribution of 0.5PbO-NG. **(c)** Nitrogen adsorption-desorption isotherm diagram and **(d)** Pore diameter distribution of 0.5CdO-NG.

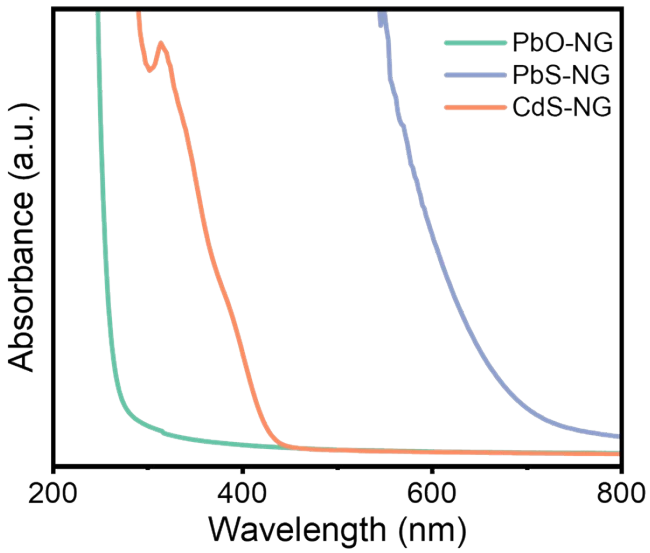

Figure S4. Absorption spectrum of PbO-NG, PbS-NG and CdS-NG.

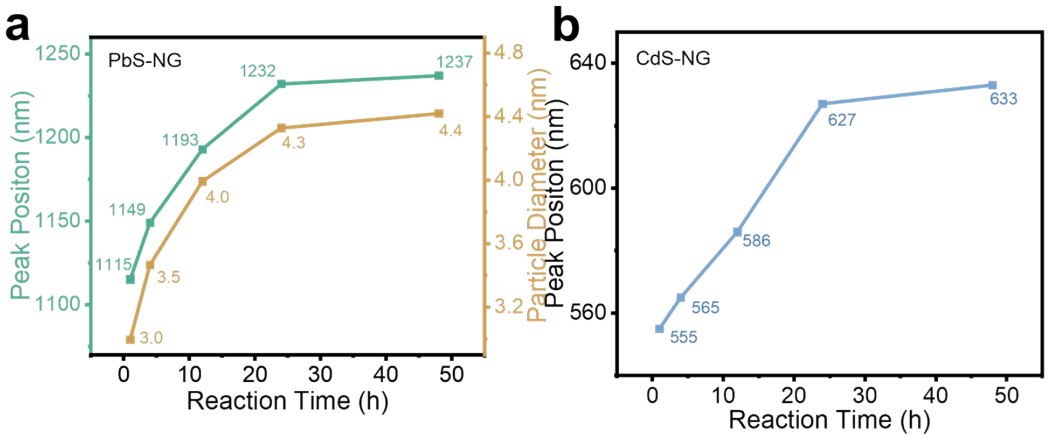

Figure S5. (a) Peak position and particle diameter of 0.5PbS-NG change with reaction time. **(b)** Peak position of 0.5CdS-NG change with reaction time.

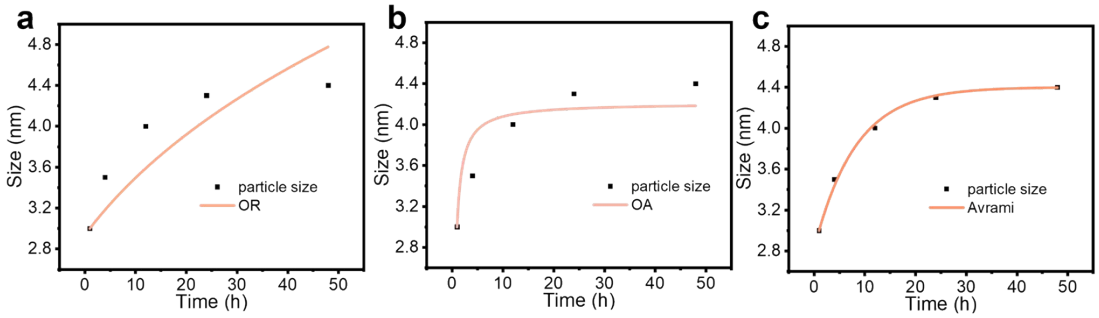

Figure S6. Experimental data and fitting results for particle sizes vs time by **(a)** OR model, **(b)** OA model and **(c)** Avrami equation

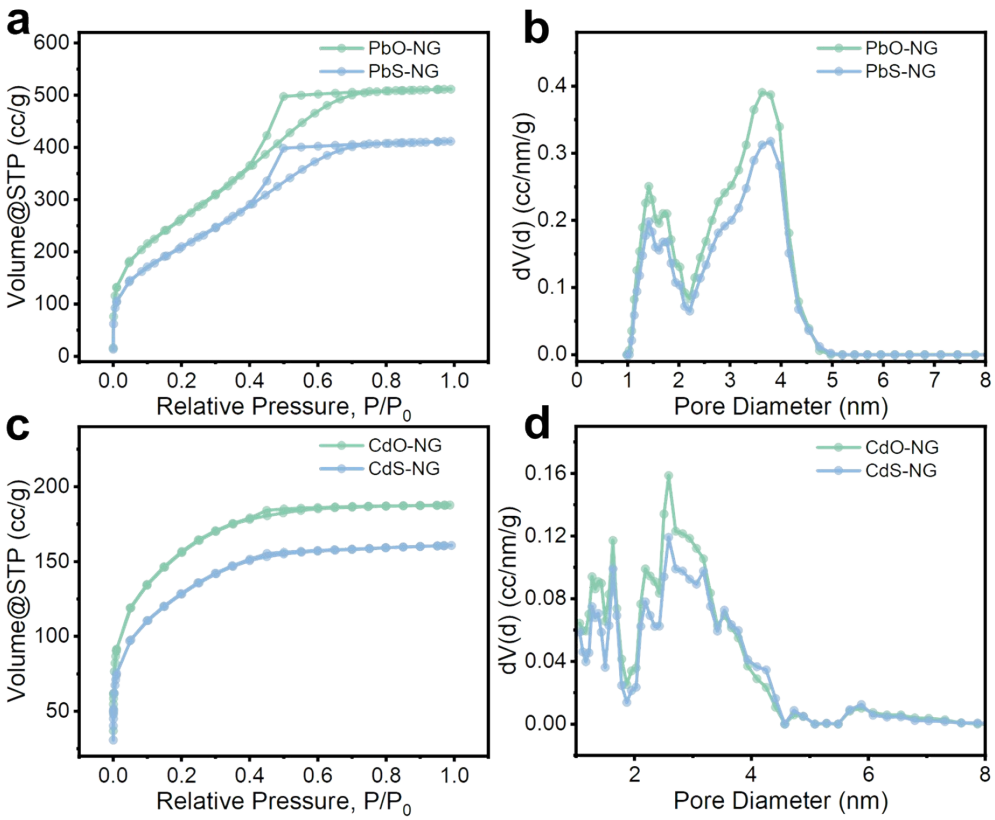

Figure S7. (a) Nitrogen adsorption-desorption isotherm diagram and **(b)** Pore diameter distribution of 0.5PbO-NG and 0.5PbS-NG. **(c)** Nitrogen adsorption-desorption isotherm diagram and **(d)** Pore diameter distribution of 0.5CdO-NG and 0.5CdS-NG.

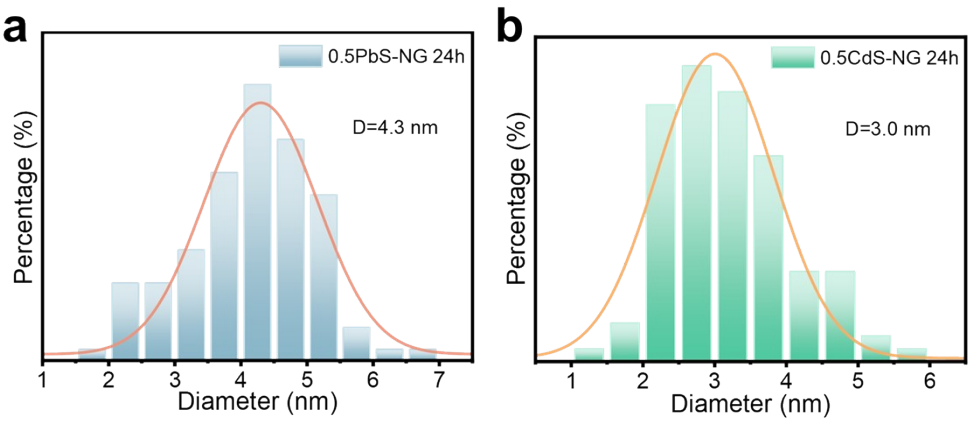

Figure S8. Size distribution histogram of **(a)** PbS QDs and **(b)** CdS QDs in corresponding glasses.

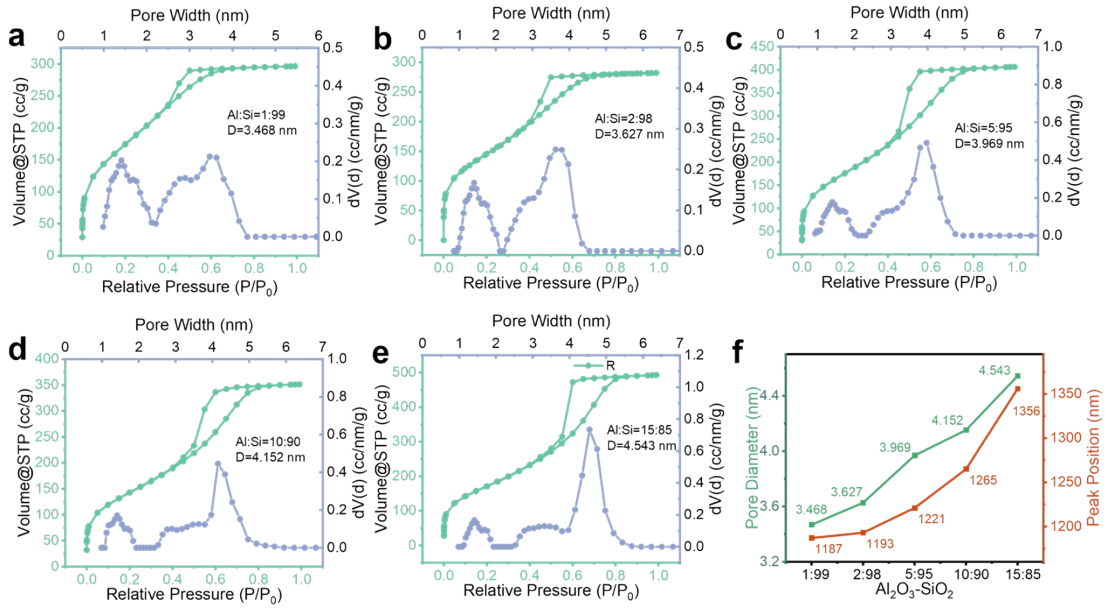

Figure S9. Pore diameter distribution and nitrogen adsorption-desorption isotherm diagram of PbO-NG with Al/Si ratio of **(a)** 1:99 **(b)**2:98 **(c)** 5:95 **(d)** 10:90 **(e)** 15:85. **(f)** PL peak position and glass pore size change with Al / Si ratio.

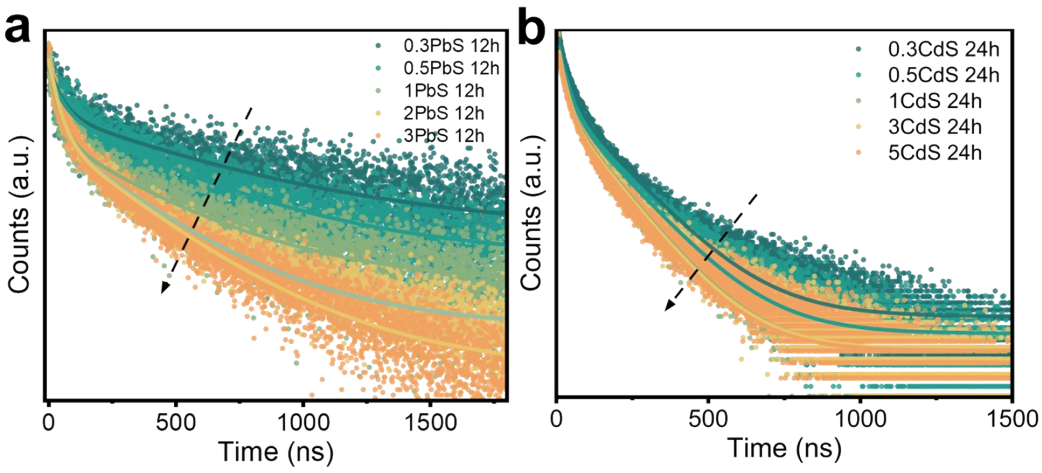

Figure S10. (a) PL decay curves of PbS-NG 12 h with different doping concentration. **(b)** PL decay curves of CdS-NG 24 h with different doping concentration.

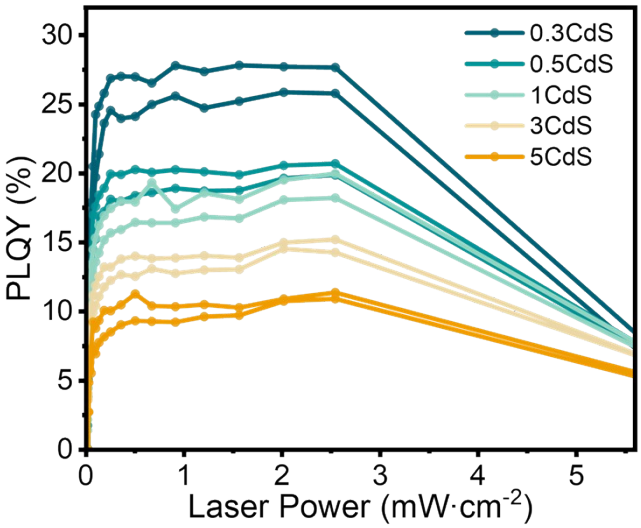

Figure S11. PLQY of 0.3/0.5/1/3 CdS-NG.

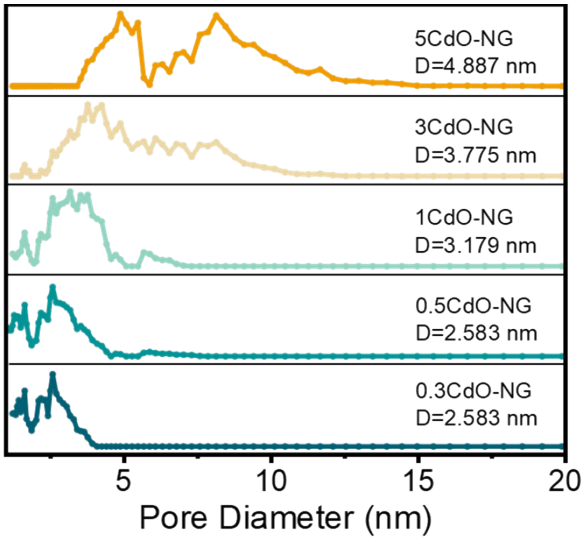

Figure S12. Pore diameter distribution of 0.3/0.5/1/3/5CdO-NG.

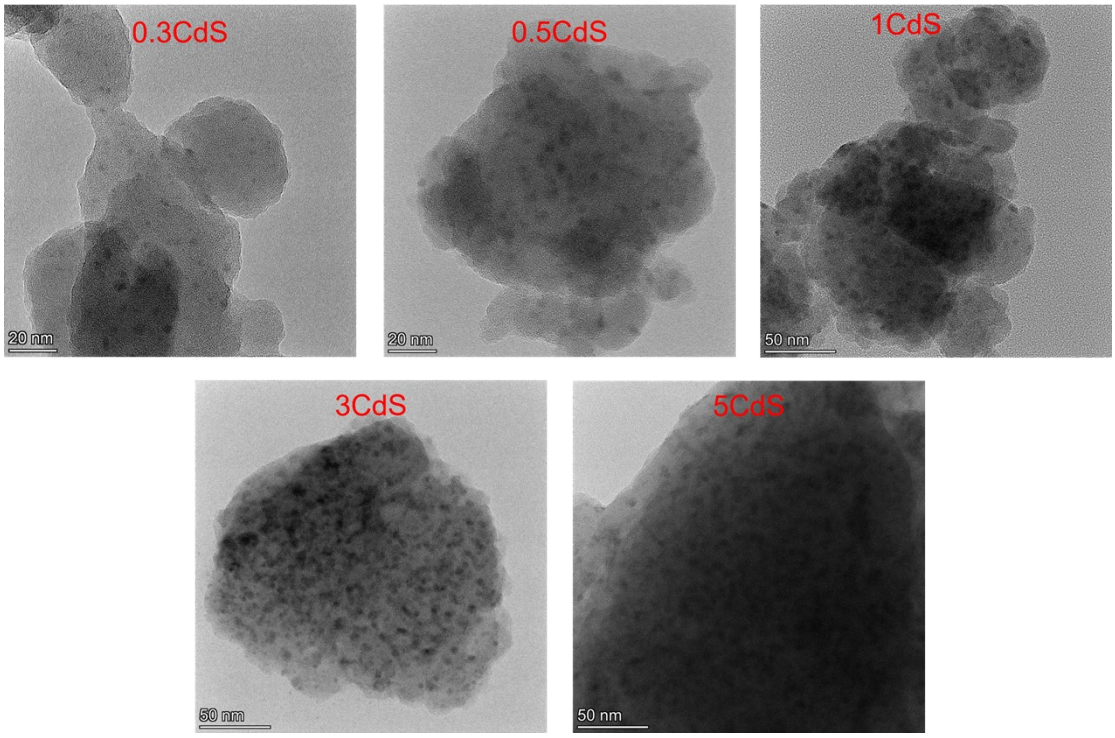

Figure S13. TEM images of 0.3/0.5/1/3/5CdS-NG.

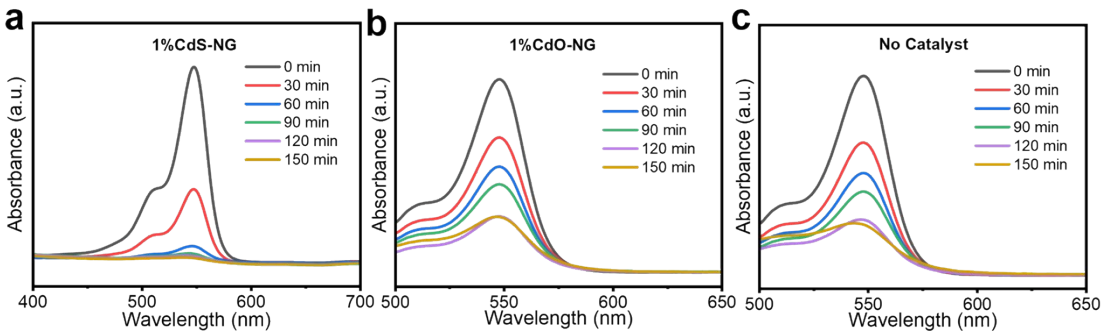

Figure S14. UV-vis absorption spectra of rose red dye solution under **(a)** CdS-NG, **(b)** CdO-NG, and **(c)** catalyst-free conditions at different reaction times

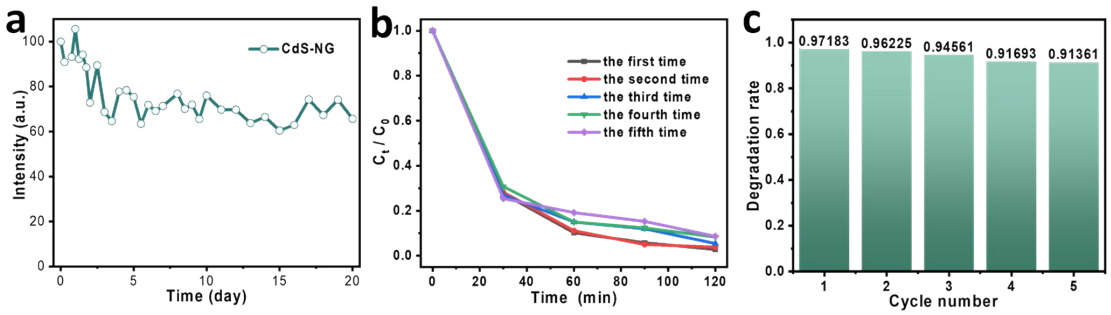

Figure S15. Stability tests of CdS-NG for **(a)** 20-day PL intensity tracking in WLED, **(b)** Cyclic degradation curves of Rose Red dye and **(c)** Degradation rates over 5 cycles in phto-catalysis.

Table S1. The summary of QDs in NG host in this work and literatures

Glass matrix	Glass preparation method	QD	QD Synthesis Method	Emission	PLQY	Life time	Interface interaction	Growth mechanism	Application	Reference
CdO-Al_2O_3-SiO_2	Sol-gel	CdS	One-step RT gas-phase method	587-689 nm	25%	93-118 ns	chemical bonding	Y	WLED/Photocatalysis	This work
PbO-Al_2O_3-SiO_2	Sol-gel	PbS	One-step RT gas-phase method	1176-1356 nm	/	363-805 ns	chemical bonding	Y	/	This work
Al_2O_3-SiO_2	Sol-gel	$CsPbX_3$	CVD	450-650 nm	70%	5.05 ns	chemical bonding	Y	WLED	[1]
Al_2O_3-SiO_2	Sol-gel	$CsPbX_3$	Two-step liquid phase method	420-630 nm	/	34.25 ns	/	/	LED sensor	[2]
PbO-Al_2O_3-SiO_2	Sol-gel	PbS	One-step liquid phase method	1250-1580 nm	/	0.71-4.93 μs	/	/	Optical communication	[3]
Al_2O_3-SiO_2	Sol-gel	$MAPbBr_3$	Two-step liquid phase method	450-770 nm	85%	4.3 ns	chemical bonding	Y	LED gas sensor	[4]
XO-Al_2O_3-SiO_2 (M= Pb, Cd, Zn, Ag)	Sol-gel	$CsPbX_3$, CdS, CdSe, CdTe, PbS, PbSe, ZnS, $AgInS_2$, Ag_2S	One-step liquid phase method	380-1600 nm	82%	16-699 ns	chemical bonding	Y	3D printing photonic and optical devices	[5]
Al_2O_3-SiO_2	Sol-gel	Carbon dot	Sintering at 500 -700 °C	500-550 nm	50.20%	548 ms	chemical bonding	/	Afterglow materials	[6]
$AlPO_4$	Sol-gel	PbS	Impregnation method	1090-1350 nm	/	/	/	/	Nonlinear optics	[7]

Glass matrix	Glass preparation method	QD	QD Synthesis Method	Spectrum	PLQY	Life time	Interface interaction	Growth mechanism	Application	Reference
SiO_2	Heat-treatment induced phase separation	$CsPbX_3$	Impregnation method	440-620 nm	28%	3.47 ns	/	/	/	[8]
$CdO\text{-}SiO_2$	Sol-gel	CdS	One-step RT gas-phase method	/	/	/	/	/	/	[9]

Discussion on the Growth kinetics of QDs in NGs

In order to further investigate the growth kinetics of quantum dots (QDs) in nano-confined glass matrix, various classical crystal growth kinetic models, including Oswald ripening (OR) [10], orientation attachment (OA) [10, 11] and Avrami equations [12-14], were applied to discuss the growth kinetics of QD in nano-confined glass matrix. OR, OA and Avrami equations as shown Equation 1, 2 and 3 were applied to fit the size growth of PbS QDs in glass pores.

$$D_t^{\,n} - D_0^{\,n} = k_1(t - t_0) \quad \text{(OR)} \qquad \text{Equation 1}$$

$$D_t = \frac{D_0(\sqrt[3]{2}k_2 t + 1)}{k_2 t + 1} \quad \text{(OA)} \qquad \text{Equation 2}$$

$$\frac{D_t - D_0}{D_m - D_0} = 1 - e^{-k(t - t_0)} \quad \text{(Avrami)} \qquad \text{Equation 3}$$

Where D_t is the particle size at time t, D_0 and t_0 are the initial size and time, n is an exponent relevant to the coarsening mechanism, D_m is the maximum diameter, and k_1, k_2 and k_3 are the rate constants.

According to the fitting results in Fig. S5, OR and OA model have obvious deviations in describing the entire growth process of QDs, which is attributed to the following factors. Firstly, OR and OA model are kinetic models to describe inter-particle coarsening that is the late stages of crystal growth or after phase transformation completes. Secondly, the OR model describes the dissolution of small particles and the deposition of large particles in the liquid or molten system, while the OA model emphasizes the orientation polymerization of nanocrystals along the crystal plane in the solution [1]. In contrast, our system is a gas-solid interface reaction, and the ions diffuse locally to generate quantum dots, and thus the growth mechanism is inconsistent with the OA and OR model hypothesis.

It is interesting to discover Avrami equation could reflects growth kinetics of QDs in nano-confined glass pores as shown in Fig.S5c to describe the growth rate decays exponentially until saturation as the reaction proceeds. The Avrami Equation is a

fundamental kinetic model to describe the time-dependent transformation of a material from one phase to another, such as during crystallization from a melt or a glass. The model incorporates both nucleation (the formation of new stable particles) and growth (their subsequent expansion) into a single expression and provides crucial insight into the mechanism of the transformation, quantifying the fraction of the new phase induced by the solid reactions over time under isothermal conditions [3, 4]. The agreement between Avrami equation and QDs growth governed by the gas-solid diffusion process and limited by pore geometry indicates the possibility that Avrami model may be applied to quantitatively elaborate confined growth processes. The characteristic sigmoidal "S-shaped" curve in Avrami is highly consistent with the observed changes of quantum dot size and photoluminescence wavelength over time. However, further studies are necessary to verify this agreement and fully elucidate the mechanistic details of nanoconfined growth, such as pore structure effects and reactant transport dynamics.

Reference

[1] Wang P, Hu Z, Cong P, et al. Spatial and chemical dual nano-confined ultrastable perovskite quantum dots glass manifesting exciton modulation. Advanced Optical Materials, 2024, 12(21): 2400630. DOI: 10.1002/adom.202400630.

[2] Hu Z, Jiang Y, Zhou F, et al. Nano-confined growth of perovskite quantum dots in transparent nanoporous glass for luminescent chemical sensing. Advanced Optical Materials, 2023, 11(4): 2202131. DOI: 10.1002/adom.202202131.

[3] Chen J, Chen C, Lau K Y, et al. Nanoconfined synthesis of lead sulfide quantum dots embedded in mesoporous aluminosilicate glass with adjustable near-infrared broadband luminescence. Chemistry of Materials, 2024, 36(3): 1113. DOI: 10.1021/acs.chemmater.3c01076.

[4] Feng K, Zhou F, Wang C, et al. Ultra-rapid and reusable luminescent gas sensor based on MAPbX3 quantum dots nano-confined in glass. Advanced Photonics, 2026, 8(1): 016006-016006. DOI:10.1117/1.AP.8.1.016006.

[5] Zhou F, Yang Y, Feng K, et al. 3D Printing of glasses with tunable UV–VIS–IR photoluminescence via low-temperature nanoscale engineering. Nat Commun (2026). https://doi.org/10.1038/s41467-026-68523-z.

[6] Wang P, Cong P, Chen J, et al. Glass-confined carbon dots: transparent afterglow materials with switchable TADF and RTP. Nanoscale, 2025, 17(15): 9144-9153.

DOI: 10.1039/d4nr04835k.
[7] Bai Z, He J, Wang Y, et al. Colloidal PbS quantum dot-$AlPO_4$ nanoporous glass composites: Controllable emission and nonlinear absorption. Journal of Luminescence, 2017, 192: 675-683. DOI: 10.1016/j.jlumin.2017.07.043.
[8] Han Y, Sun J, Ye S, et al. A stimuli responsive material of perovskite quantum dots composited nano-porous glass. Journal of Materials Chemistry C, 2018, 6(41): 11184-11192. DOI: 10.1039/c8tc04383c.
[9] Nogami M, Nagasaka K, Takata M. CdS microcrystal-doped silica glass prepared by the sol-gel process. Journal of non-crystalline solids, 1990, 122(1): 101-106. DOI: 10.1016/0022-3093(90)90231-A.
[10] Zhang J, Huang F, Lin Z. Progress of nanocrystalline growth kinetics based on oriented attachment. Nanoscale, 2010, 2(1): 18-34. DOI: 10.1039/b9nr00047j.
[11] Huang F, Zhang H, Banfield J F. The role of oriented attachment crystal growth in hydrothermal coarsening of nanocrystalline ZnS. The Journal of Physical Chemistry B, 2003, 107(38): 10470-10475. DOI: 10.1021/jp035518e.
[12] Liu L, Long Z, Shi K, et al. A general crystallization picture of quantum dots: the underlying physical chemistry. CCS Chemistry, 2025, 7(4): 926-949. DOI: 10.31635/ccschem.024.202404892.
[13] Jia J, Iwasaki S, Yamamoto S, et al. Temporal evolution of microscopic structure and functionality during crystallization of amorphous indium-based oxide films. ACS Applied Materials & Interfaces, 2021, 13(27): 31825-31834. DOI: 10.1021/acsami.1c05706.
[14] Doblas D, Rosenthal M, Burghammer M, et al. Smart energetic nanosized co-crystals: exploring fast structure formation and decomposition. Crystal Growth & Design, 2016, 16(1): 432-439. DOI: 10.1021/acs.cgd.5b01425.